Originally published as:

Kaveh Mollazade ; Mahmoud Omid ; Fardin Akhlaghian Tab ; Yousef Rezaei Kalaj ;
Seyed Saeid Mohtasebi ; Manueal Zude : Analysis of texture based features for predicting mechanical properties of horticultural products by laser light backscattering imaging .
in: Computers and Electronics in Agriculture 98 (2013) 10 S. 34-45

DOI: 10.1016/j.compag.2013.07.011

Analysis of texture-based features for predicting mechanical properties of horticultural products by laser light backscattering imaging

Kaveh Mollazade [a *], Mahmoud Omid [a], Fardin Akhlaghian Tab [b], Yousef Rezaei Kalaj [c], Sayed Saeid Mohtasebi [a], Manuela Zude [c]

[a] Department of Agricultural Machinery Engineering, Faculty of Agricultural Engineering and Technology, University of Tehran, P.O. Box 4111, Karaj 31587-77871, Iran

[b] Department of Computer Engineering, Faculty of Engineering, University of Kurdistan, Sanandaj, Iran

[c] Leibniz Institute for Agricultural Engineering Potsdam-Bornim (ATB), Max-Eyth-Allee 100, 14469 Potsdam, Germany

[*] Corresponding author; Tel: +98 918 9720639; Fax: +98 261 2808138
E-mail address: mollazade@ut.ac.ir (K. Mollazade)

Abstract

Light backscattering imaging is an advanced technology applicable as a non-destructive technique for monitoring quality of horticultural products. Because of novelty of this technique, developed algorithms for processing this type of images are in preliminary stage. Texture is one of the most important characteristics of images and has been used widely in agro-food industry for assessing qualitative properties of different types of products. The present study investigates the feasibility of texture-based features to develop better models for predicting mechanical properties (fruit flesh firmness or elastic modulus) of horticultural products. Images of apple, plum, tomato, and mushroom were acquired using a backscattering imaging setup capturing 660 nm. After segmenting the backscattering regions of images by variable thresholding technique, they were subjected to texture analyses and space domain techniques in order to extract a number of features. Adaptive neuro-fuzzy inference system models were developed for firmness or elasticity prediction using individual types of feature sets and their combinations as input for prediction model applicable in real-time applications. Results showed that fusion of the selected feature sets of image texture analysis and space domain techniques provide an effective means for improving the performance of backscattering imaging systems in predicting mechanical properties of horticultural products. The maximum value of correlation coefficient in the prediction stage was achieved as 0.887, 0.790, 0.919, and 0.896 for apple, plum, tomato, and mushroom products, respectively.

Keywords: ANFIS, backscattering, feature fusion, quality evaluation, texture analysis.

1. Introduction

Fruit flesh firmness and elastic modulus are two main mechanical parameters in determining maturity and harvest time of horticultural products, and they are also key parameters in evaluation and grading postharvest quality of fruit and some vegetables. Mechanical properties of fresh produce change during growth and storage processes. The conventional standard methods, like Magness-Taylor compression test and Youngs' modulus of elasticity, are not suitable for real-time applications, such as grading and sorting machines, because the samples should be per definition or potentially damaged during the test. Technical advances over the last few decades considering spectrophotometers, multi- and hyperspectral systems as well as computer vision systems have led to the development of non-destructive devices capable of measuring internal qualitative parameters of horticultural products. Garcia-Ramos et al. (2005) reviewed the non-destructive techniques developed to measure mechanical properties of agricultural products. They concluded that optical techniques have the advantage over the others, since they can estimate several internal variables, such as sugar content, acid content, firmness, and elasticity, with a single sensor. However, it has been shown that the application of spectroscopic analyses is not capable to build robust calibrations for predicting the mechanical properties of the produce, while the composition considering pigments, soluble solids content, dry matter, and moisture content as well as the detection of internal physiological disorders appeared feasible in several products (Zude, 2009).

As an optical technique, computer vision-based quality evaluation systems are being used increasingly in the agro-food industry because of their rapid, non-contact, and non-destructive manner as well as availability of inexpensive camera systems. Driven

by considerable improvements in imaging hardware and rapid progression in image processing techniques, computer vision has established its applications for the internal surveillance of both fresh and processed agro-food materials. In combination with multi- or hyperspectral imaging more specific variation of the produce, such as the detection of distribution of water core and internal browning has been shown.

Horticultural products, as biological materials, are supposed to be turbid and transmit the light through the tissue depending on the wavelengths (Mireei, 2010). When light source impinges to a biological tissue, its internal contents reflect most of the passing light as scattering photons towards the exterior tissue surface. Due to physiochemical properties of the tissue, photons are scattered at different angles, leading to their stochastic interaction with the internal components of biological tissue like joint surfaces of the cell wall, chloroplasts, mitochondria, etc (Nicolai et al., 2007). Because of this interaction, backscattering photons carry information related to the morphology and structures of the tissue, such as mechanical properties additionally to the information on absorbing molecules. Few work groups showed that it is possible to record backscattered photons by a camera equipped with an imaging sensor sensitive in the range of visible and short wave near infrared (SWNIR) of electromagnetic spectrum. The technique focuses on the processing of these types of images and extracting knowledge from them has been named as backscattering imaging. Based on the light source and imaging unit used, the technique is divided into three categories: hyperspectral backscattering imaging (HBI), mutispectral backscattering imaging (MBI), and laser light (monochromatic) backscattering imaging (LLBI). The acquired images by these categories are similar, when we speak about a certain wavelength (Mollazade et al., 2012a).

In most researches done to date, light intensity-based features in the space domain were used to establish calibration models between the backscattering images and reference physical properties. Qing et al. (2007) used the simplest type of features, i.e. the area of backscattering region that is equal to the total number of pixels in the segmented backscattering image, to predict firmness of apple. Another simple technique is to use the mean intensity value (Qing et al., 2008) or some statistical characteristics of pixels remained after segmenting the backscattering region (Noh and Lu 2007). Lu (2004) introduced a method, known as radial averaging, in which scattering region of photons is divided into several circular rings and then average value of all pixels within each ring is recorded as the features of image. Using the radial averaging approach, researchers applied different semi-Gaussian mathematical functions, like exponential, Lorentzian, and Gompertz, to fit one-dimensional (1D) scattering profiles as a function of distance. The values of parameters of the fitted functions were then used as the features of images (Peng and Lu 2005, 2006, 2007). Extracting the absorption and reduced scattering coefficients of 1D profile from the Farrell's diffusion theory model is another method used to predict firmness of apple (Qin and Lu, 2006).

Although the above mentioned techniques have shown relatively fair utility in describing the backscattering features, their relative performance in predicting mechanical properties of horticultural products is not quite clear because they were tested in separate studies, where the samples used were different and the experimental setups were not the same. Hence, direct comparison of these feature extraction techniques is required in order to investigate which method is the most suitable for predicting mechanical properties of horticultural products. Furthermore, previous techniques are based on some simple statistical features of pixel brightness or analysis

of 1D scattering profiles, and they did not investigate the pixel intensity pattern from the overall two-dimensional (2D) scattering images acquired at a specific wavelength. Use of 2D processing algorithms could present a chance to improve the performance of backscattering imaging technique in predicting firmness and elasticity of horticultural produce. Texture, as a 2D processing approach, is an important image feature that corresponds to both brightness value and pixel locations. Many researchers reported the feasibility of texture-based features in the food industry for quality evaluation and inspection (Jackman and Sun, 2012). The distribution pattern of backscattering photons is unique for each backscattering image, since the spatial pattern in an image reflects the physiochemical properties of a product. Hence, by utilizing the texture-based features, researchers may improve the accuracy performance and take feasibility of backscattering systems in real-time applications.

Therefore, the overall objective of this research was to use LLBI technique for predicting firmness and elastic modulus (elasticity) of a wide range of horticultural products. The specific objectives were to:

- Analysis the capability of different texture processing techniques for firmness/elasticity prediction.
- Compare the texture-based feature extraction techniques with those reported in the previous researches (space domain techniques).
- Establish intelligent models for firmness/elasticity prediction by adaptive neuro-fuzzy inference system (ANFIS).
- Suggesting the best feature set for real-time applications.

2. Materials and methods

2.1. Data set

Mechanical properties obtained from two stony fruits (apple and plum), a non-stony fruit (tomato), and a vegetable (mushroom) were used as data set. Harvested manually from the garden and greenhouse, samples were visually inspected for appearance and surface defects. Only those samples free of visual defects (such as scars, cuts, shrivel, etc.) were selected for the experiments. To generate samples with variations in their properties, they were separated into several groups and stored at the standard temperature and relative humidity conditions. Groups of samples were withdrawn from the storage chamber two hours before the experiments at regular intervals of 15, 3, 7, and 3 days for apple, plum, tomato, and mushroom, respectively. After acquisition of backscattering images, samples were subjected to compression test. Firmness was measured as the mechanical signature of stony fruits, while for tomato and mushroom samples, elasticity was calculated (Mohsenin, 1986). Table 1 summarizes some information related to the samples, measurement conditions, and mechanical tests.

Table 1.

2.2. Backscattering image acquisition

Backscattering images were acquired using an in-house built LLBI system (Baranyai and Zude, 2009). The system mainly consisted of a wide dynamic range monochrome CCD camera (JAI A50IR CCIR, JAI, Denmark) with a zoom lens (model H6Z810, PENTAX Europe GmbH, Germany), a solid-state laser diode emitting at 660 nm as the light source (LPM series, Newport Corp., USA), a laser driver, a sample holder unit, video converter (VRM AVC-1, Stemmer Imaging GmbH, Germany), and a

computer equipped with an in-house developed software to acquire the backscattering images. The backscattering images with the spatial resolution of 720×576 pixels were acquired in a dark room and laser diode spot of 1 mm diameter provided an acceptable signal to noise ratio. The camera was placed perpendicular to the sample holder while the incident angle of the laser beam was adjusted to 15º.

2.3. Image processing

Image processing was carried out using MATLAB R2009a and its image processing toolbox (The Mathworks, Inc., Natick, MA, USA).

2.3.1. Segmentation

Segmentation plays a key role in processing of backscattering images. If it does not perform well, useful information may be omitted. Segmentation operation consists of segregating the region of interest (ROI), backscattering photons minus those saturate the CCD of camera, from the background. This operation was carried out in two steps as following:

1. Removing saturated pixels: Since saturated region in images consists of photons that directly return to the camera's sensor, the light intensity of pixels in this region is close to its maximum value, i.e. 255. By a trial and error procedure, it was found that saturated regions are segmented successfully by the static threshold value of 252.

2. Segmenting regions consists of backscattering photons from the background: Variable thresholding by local statistics is a powerful segmentation technique when background illumination is uneven. At each pixel of image, the threshold value is defined based on some statistical features extracted from the neighborhood pixels (Gonzalez and Woods, 2004). In the current study, threshold values were selected

based on the standard deviation and the average of a 3×3 neighborhood for each pixel. These features were very useful in setting local thresholds, because they are contrast and average of local intensity.

2.3.2. Texture analysis

A wide variety of techniques have been proposed for describing image texture (Zheng et al., 2006). Approaches to texture analysis are usually classified into four categories: statistical, structural, transform-based, and model-based. Statistical techniques represent the texture indirectly by non-deterministic properties that govern the distribution and relationship between the grey levels of an image. Structural approaches represent texture through some structural primitives constructed from grey values of pixels. In the transform methods of texture analysis, an image is represented in a space whose co-ordinate system has an interpretation that is closely related to the characteristics of a texture (such as frequency or size). Model-based texture analysis attempts to interpret an image texture by use of, respectively, generative image model and stochastic model. The parameters of the model are calculated, based on the relationship of the grey values between a pixel and its neighboring pixels, and then these are used for image analysis.

To process backscattering images, texture-based features from four statistical techniques (first order statistics of image histogram (FOSH), grey level co-occurrence matrix(GLCM), grey level run length matrix (GLRLM), and local binary pattern (LBP)), three transform-based techniques (wavelet transform, Gabor transform, and Tamura), and two model-based techniques (fractal model and simultaneous autoregressive model), were considered. Structural techniques were not considered in this research since the structural primitives used in these methods can only describe

very regular textures (Bharati et. al.,2004). Furthermore, structural techniques are rarely used in the food industry to describe texture characteristics (Zheng et al., 2006). A brief description of these techniques is provided in the following subsections.

2.3.2.1. First order statistics of image histogram

First order statistics of image histogram are considered as the most basic feature extraction method of image texture. They act based on the probability of occurring pixel intensity values in the image. They depend only on individual pixel values and not on interaction of neighboring pixel values. First the histogram of grey level backscattering images was extracted. The histograms were then normalized according to the following formula:

$$p(z_i) = \frac{H(z_i)}{N_I} \quad (1)$$

where $H(z_i)$ is the image histogram, $p(z_i)$ is the normalized histogram, and N_I is the total number of arrays in the image matrix. Using the normalized histogram and relations based on the occurrence of grey levels, eight statistical features were extracted from each backscattering image (Bevk and Kononenko, 2002). The list of features is presented in Table 2.

2.3.2.2. Grey level co-occurrence matrix

A GLCM is a matrix in which grey level pixels are considered in pairs with a relative distance d and orientation θ among them. The entry $G_{d\theta}(i, j)$ of this matrix is the number of occurrences of a pair of grey levels, i and j, for the specified displacement. The scattering images were analyzed using the distance d=1 pixel with angles θ = 0, 45, 90, and 135° as suggested by Haralick (1979). After calculating GLCMs, they were normalized so that sum of arrays in the normalized matrix is equal to 1. Ten

features were then extracted from each normalized GLCM according to Table 2 (Haralick et al., 1973). Thus, a total of 40 features (4 orientations × 10 statistical features) were extracted from each image.

2.3.2.3. Grey level run length matrix

Run length technique records the coarseness of a texture in specified directions by encoding textural information based on the number each grey level appearing in the image by itself. A run is defined as a string of consecutive pixels which have the same grey level intensity along a specific linear orientation. Fine textures tend to contain more short runs with similar grey level intensities, while coarse textures have more long runs with significantly different grey level intensities. A GLRLM is a matrix in which each element $r(i,j)$ determines the total number of occurrence of run lengths j in the grey level i in specified direction θ. Run length matrices at four directions θ = 0, 45, 90, and 135º were extracted for each backscattering image. Once the GLRLMs were calculated along each direction, 11 texture descriptors, as suggested by Tang (1998), were calculated to capture the texture properties and differentiate among different textures (Table 2). For each image, a total of 44 features (11 GLRLM texture descriptors × 4 directions) were obtained.

2.3.2.4. Local binary pattern

The LBP texture analysis operator is defined as a grey-scale invariant texture measure, derived from a general definition of texture in a local neighborhood. For each pixel in an image, a neighborhood of the image (usually a 3 × 3 window) is considered and the intensity value of neighboring pixels is compared with that of the central pixel. If the intensity value of neighboring pixels is greater or equal to the

central pixel value, they are replaced with ones. Otherwise, their value is zero. Finally, central pixel is replaced with the binary weighted sum of neighboring pixels and the neighboring window is transferred to the next pixel. The output of LBP operator is a P-bit binary number (P is the number of neighboring pixels), which can take 2^P different values. Furthermore, LBP is completely dependent to indexing of pixels contained in the neighborhood. Thus, in order to assign a unique value to each private binary pattern, LBP matrices were robust to rotation by clockwise rotation of the obtained binary number and selecting the maximum possible value (Ojala et al., 2002). Finally, 8 statistical features were extracted from the normalized histogram of GLRLM of each backscattering image.

2.3.2.5. Wavelet transform

Wavelet transform is a useful tool for analyzing the texture of agricultural materials. A discrete wavelet transform (DWT) decomposes an image onto multiple wavelet components using a filter bank as suggested by Mallat (1989). It provides four sets of coefficient at each level of decomposition. Rows of the input image are first passed through the low and high pass filters, followed by down-sampling along the rows by a factor of 2. The columns of resulting images from both filters are sent through low and high pass filters followed by down sampling along the columns to obtain four sets of coefficients; namely, approximation, horizontal, vertical, and diagonal details (Choudhary et al., 2008). Backscattering images were subjected to six levels of wavelet decomposition using a fourth-order Daubechies mother wavelet (Db4), which is the most popular mother wavelet family for image texture analysis. At each level of decomposition, approximation coefficients and wavelet detail coefficients were obtained for horizontal, vertical, and diagonal orientations. To determine optimum

level of decomposition, backscattering images at each level of decomposition were compared to the original images. As is shown in the Figure 1, an increase in the levels of decomposition leads to increase the amount of down-sampling, resulting in lower resolutions at successive levels. So, the wavelet coefficients from first to the fourth level of decomposition were considered to be used in feature extraction stage. Four statistical descriptors including mean, standard deviation, energy, and entropy were extracted from each level of decomposition. A total of 64 features (4 statistical descriptors × 4 wavelet coefficients × 4 decomposition levels) were obtained from the DWT of each backscattering image.

2.3.2.6. Gabor transform

Gabor transform is one of the most effective and most popular filter-based approaches to extract texture features of an image. Gabor filter is obtained by multiplying a Gaussian function in a directional sine function. Therefore, this filter generates powerful responses at locations with specific local direction and frequency (Zhu et al., 2007). Gabor wavelet is a kind of wavelet transform function in which its mother wavelet is a Gabor filter. After applying the Gabor wavelet on backscattering images, a new matrix with M×N dimension was obtained. Each dimension represents a frequency in a specific direction. Since each element of the final image, after applying the Gabor transform, is a complex number with both real and imaginary parts, the matrix magnitude was used for feature extraction (Figure 2). Mean, standard deviation, energy, and entropy were used as statistical descriptors in order to build the feature vector containing the texture descriptors of backscattering images by Gabor filter. These statistical operators were then applied on the magnitude of matrices found in the previous section for each backscattering image in four frequencies

(0.1768, 0.25, 0.3536, and 0.5 Hz) and four directions (0, π/4, π/2, and 3π/4 radian). The size of feature vector based on the Gabor transform was 64 (4 statistical descriptors × 4 frequencies × 4 directions).

2.3.2.7. Tamura

Tamura features are designed based on psychological studies on human visual perception of objects texture (Tamura et al., 1978). These features include coarseness, contrast, directionality, line-likeness, regularity, and roughness. Since the last three features are derived from the first three ones, only coarseness, contrast, and directionality just were extracted from each backscattering image.

An image contains textures at several scales; coarseness aims to identify the largest size at which a texture exists, even though a smaller micro texture may exist. To compute the coarseness, using a $2^k \times 2^k$ (k=0,1,…,5) window, first a moving average filter $A_k(x,y)$ was applied on each pixel:

$$A_k(x,y) = \sum_{i=x-2^{k-1}}^{x+2^{k+1}-1} \sum_{j=y-2^{k-1}}^{y+2^{k+1}-1} \frac{g(i,j)}{2^{2k}} \quad (2)$$

where $g(i,j)$ is the intensity value at pixel (i,j).

Then at each pixel differences between pairs of $A_k(x,y)$ corresponding to non-overlapping neighborhoods on opposite sides of the point in both horizontal and vertical orientations were calculated:

$$E_{k,h}(x,y) = |A_k(x + 2^{k-1}, y) - A_k(x - 2^{k-1}, y)| \quad (3)$$

$$E_{k,v}(x,y) = |A_k(x, y + 2^{k-1}) - A_k(x, y - 2^{k-1})| \quad (4)$$

In order to determine the filter window size for each pixel which gives the highest output value, the value of k was taken in which E is maximized in either direction. The coarseness was then computed by the following formula:

342 $$F_{crs} = \frac{1}{m \times n} \sum_{i=1}^{m} \sum_{j=1}^{n} 2^k(i,j) \quad (5)$$

343 Contrast aims to capture the dynamic range of grey levels in an image, together with
344 the polarization of the distribution of black and white. The first is measured using the
345 standard deviation of grey levels (σ) and the second from the kurtosis α_4. The contrast
346 measure was therefore defined as:

347 $$F_{con} = \frac{\sigma}{\alpha_4^{1/4}} \quad (6)$$

348 Directionality is a measure of the orientation of the image grey values. To compute
349 the directionality, initially two simple masks were used first to detect edges in
350 backscattering images. At each pixel the angle and magnitude were calculated. A
351 histogram of edge probabilities was then built up by counting all points with
352 magnitude greater than a threshold and quantizing by the edge angle. The histogram
353 reflects the degree of directionality. Finally, the directionality was then computed
354 from the sharpness of the peaks of histogram using their second moments.

355

356 2.3.2.8. Fractal model

357 In the image analysis of agro-food materials, fractal dimension can be used to
358 estimate and quantify the complexity of the shape or texture of images. The fractal
359 dimension gives a measure of the roughness of an image. Intuitively, the larger the
360 fractal dimension, the rougher the texture is (Zheng et al., 2006). There are a number
361 of methods proposed for defining the fractal dimensions, where the most common one
362 is the Hausdorff's dimension (D_0):

363 $$D_0 = lim_{\varepsilon \to 0} \frac{log\, N(\varepsilon)}{log\, \varepsilon^{-1}} \quad (7)$$

364 where $N(\varepsilon)$ is the number of hypercubes of Euclidean dimension E, and length ε that
365 fill the object. In this research, a new developed algorithm known as segmentation-

366 based fractal texture analysis (SFTA) was used to extract the Hausdorff's fractal
367 dimension of backscattering images (Costa et al., 2012). The SFTA algorithm was
368 implemented in two steps. In the first step, a set of threshold values was computed
369 using multi-level Otsu algorithm and distribution of grey levels in the input images.
370 The number of optimum thresholds was set to 8, as suggested by Costa et al. (2012).
371 After that, the grey level backscattering images were disintegrated into a set of binary
372 images by selecting pairs of thresholds from the threshold set and applying the two-
373 threshold binary decomposition (TTBD) algorithm. The number of resulting binary
374 images was 16. Figure 3 illustrates the decomposition of a backscattering image taken
375 from a tomato sample at 660 nm using the TTBD algorithm. The threshold set for this
376 sample was as T=[0, 0.0039, 0.0391, 0.1367, 0.2188, 0.3477, 0.4961, 0.6914]. In the
377 second step of SFTA, Hausdorff's dimension was computed from the borders of each
378 binary image by applying the box counting algorithm (BCA). In the BCA, binary
379 images were divided into a grid composed of squares of size $\varepsilon \times \varepsilon$. The number ($N(\varepsilon)$)
380 of squares of size $\varepsilon \times \varepsilon$ that contains at least one pixel of ROI was counted. A $log\ N(\varepsilon)$
381 versus $log\ \varepsilon^{-1}$ curve was drawn for each binary image by varying the value ε. The
382 curve was approximated by a straight line using the least squares fitting approach.
383 Then, the slop of this line was recorded as the Hausdorff's dimension of each binary
384 image. The size of fractal feature vector for each backscattering image was 16 (Figure
385 3).
386
387 2.3.2.9. Autoregressive model
388 Simultaneous autoregressive (SAR), as a model-based texture analysis technique, has
389 found many applications in image segmentation (Sukissian, 1994, Sukissian et al.,
390 1997). This model acts based on the spatial relationship between the pixels of an

image. It assumes that intensity of pixels is the weighted sum of intensity from the neighboring pixels. In fact a SAR models the relationship between a pixel and its neighboring pixels using the following linear combination (Jain, 1989):

$$f(s) = \mu + \sum_{q \epsilon N} \theta(q) f(q) + \varepsilon(q) \quad (8)$$

where *f(s)*, *f(q)*, μ, $\varepsilon(q)$, *N*, and $\theta(q)$ are image intensity at position *s*, image intensity at position *q*, bias value, noise value, number of neighboring pixels, and model parameters, respectively. In the current research, the bias value was adjusted to the average of light intensity of entire image, which was formerly normalized between 0 and 1. A Gaussian random variable with mean zero and variance σ^2 was used to adjust the noise value. The number of neighboring pixels considered was equal to four according to the pattern shown in Figure 4. For each backscattering image, a total of five SAR model features, including values of θ in four neighboring pixels together with the minimum prediction error variance, were extracted.

Table 2

Figure 1

Figure 2

Figure 3

Figure 4

2.3.3. Space domain analysis

In order to assess the effectiveness of texture analysis techniques, backscattering images were subjected to several space domain techniques proposed by researchers in literature. These techniques as described in the "Introduction" section, were:

1. Total number of pixels in the segmented backscattering region of image,

2. Statistical features of segmented backscattering region of image (mean, min, max, sum, standard deviation, and variance),

3. Radial averaging technique (25 rings with thickness of five pixels),

4. Modified Lorentzian function parameters (four parameters: a, b, c, and d),

5. Modified Gompertz function parameters (four parameters: α, β, ε, and δ), and

6. Farrell's diffusion theory model parameters (two parameters: absorption (μ_a) and reduced scattering coefficients (μ_s')).

Readers can refer to the references provided in the "Introduction" section to get more information about these techniques.

2.4. Adaptive neuro-fuzzy inference system (ANFIS)

A neuro-fuzzy system integrates the advantages of artificial neural networks (ANNs) with rule-based fuzzy inference systems (FIS). It covers the lacks of these techniques when they are used individually. ANNs are efficient structures capable of learning from examples, while fuzzy systems are suitable for uncertain knowledge representation. These hybrid technique brings learning capability of ANN to FIS. During the learning process, a number of desired input–output data pairs are used, and then parameters associated with the membership functions and rules of a Takagi-Sugeno type FIS are tuned by ANN so as to map the inputs to outputs. The computation and adjustment of these parameters is facilitated by a gradient vector, which provides a measure of how well the FIS is modeling the input/output data for a given set of parameters. From the topology point of view, ANFIS is an implementation of a representative FIS using a feed forward neural network-like structure (Jang, 1993).

The fuzzy logic toolbox of MATLAB R2009a was used to create ANFIS models (The Mathworks, Inc., Natick, MA, USA). The inputs to the models were the normalized feature sets (in the range 0 to 1) extracted from backscattering images, while the output was the firmness or elasticity of samples. ANFIS is susceptible to the curse of dimensionality when number of inputs exceeds three. The training time increases exponentially with respect to the number of fuzzy sets per input variable used. An effective procedure to reduce the dimension of the input vector is to use principal component analysis (PCA). The technique was outlined by authors previously (Omid et al., 2009 and 2010). Hence, the inputs were subjected to the PCA and only the first three principal components were fed to the ANFIS. The performance of ANFIS is highly dependent to its structure. Therefore, four significant adjustments were made in the structure of ANFIS models in order to find best one for predicting firmness/elasticity of horticultural produce. Settings include the number of membership functions (changed from 2 to 5 with step size of 1), types of input membership functions (triangular, trapezoidal, bell-shaped, Gaussian, and sigmoid), types of output membership function (constant and linear), and optimization methods (hybrid and back-propagation). Each ANFIS model with its specific setting was run 20 times and the best was defined as the one with the best overall statistical accuracy measures.

2.5. Statistical measures

To ensure the models were not over-fitted and the prediction results truly represent the model performance, the samples were first divided into three separate parts randomly. The first part (or 60% of all samples) was used for training, 15% of all samples were used for cross-validation, and the remaining samples were used for independent test or

prediction. Calibration models for firmness and elasticity were developed using ANFIS from the training samples. Cross-validation was used to supervise the training process in order to prevent the over-training. Thereafter, the calibration models were used to predict the independent part of samples. The models were evaluated using root mean squares errors for cross validation (RMSECV) and prediction (RMSEP).

$$RMSE = \sqrt{\frac{\sum_{i=1}^{n}(\hat{y}_i - y_i)^2}{n}} \quad (9)$$

where $\hat{y}_i$ is the actual value, y_i is the predicted value, and n is the number of samples in prediction or calibration stages. In addition, correlation coefficients for calibration (R_c) and prediction (R_p) were also calculated. Processing time is an important factor when we want to use a backscattering imaging system in real-time applications. For each feature extraction technique, the processing time was recorded to be used as an evaluation criterion. MATLAB codes were implemented and run in a laptop computer with this configuration: Core 2Duo CPU, 2.53 GHz, 4 GB RAM, Windows 7 OC configuration.

3. Results and discussion

3.1. Individual feature set models

The statistical measures of individual texture-based feature models for predicting firmness/elasticity of apple, plum, tomato, and mushroom by ANFIS are presented in Table 3. The best firmness prediction of FOSH technique using ANFIS for apple was the highest (R_p=0.861) followed by the Tamura (R_p=0.846)), fractal (R_p=0.826)), and wavelet (R_p=0.825)). The highest prediction accuracies for plum, tomato, and mushroom were obtained by the SAR (R_p=0.757), Gabor (R_p=0.857), and Tamura (R_p=0.839), respectively, whereas, for the same, the wavelet (R_p=0.554), GLRLM (R_p=0.675), and SAR (R_p=0.717) produced the lowest prediction performance.

Comparing to the other texture analysis techniques, Tamura and fractal provided good results for all samples leading to select them as the best texture-based techniques for analysis of backscattering images because of their consistency in firmness/elasticity prediction performance. This reflects the fact that border of segmented regions along with distribution pattern of light intensity in backscattering images are closely related to the mechanical properties of horticultural products. On the other hand, LBP in all cases was one of four techniques showed the lowest correlation with the firmness/elasticity changes. The poor performance of LBP features can be attributed to the small changes of run length values in backscattering images when mechanical properties of products change. Comparing the results obtained for apple, plum, tomato, and mushroom show that Tamura, fractal, FOSH, and GLCM are the best texture analysis methods in overall for predicting firmness/elasticity of horticultural produces when they are used as an individual feature set.

Regarding the space domain features (see Table 4), results showed that statistical, radial averaging, and Farrell's features have the highest performance in predicting firmness/elasticity of apple, plum, tomato, and mushroom compared to the other techniques. However, for all products, the lowest prediction performance was recorded for the total number of pixels technique. Lorentizan and Gompertz techniques did not show the consistency in firmness/elasticity prediction so that they presented acceptable performance for tomato fruit, while for the plum and mushroom the accuracy of these techniques was considerably low. The reason for this is that the area of backscattering region for tomato fruit was bigger than that of mushroom and plum resulting in the better fitness of 1D backscattering profile by Lorentzian and Gomperzt functions. Comparing the results obtained in the Tables 3 and 4 demonstrates texture analysis techniques provide better performance than that of

space domain techniques when they are used individually. However, the differences are very small.

Table 3

Table 4

3.2. Real-time feature set models

In real-time applications, such as grading/sorting machines, two factors are important: prediction accuracy and processing time. To compare the capability of different texture and space domain techniques for real-time applications, processing time during implementation and feature extraction process for each technique was recorded. Figures 5 and 6 illustrate, respectively, the time achieved by various texture and space domain methods on the study data set, respectively. Results show that the type of sample has no significant impact on the processing time because the image dimensions are the same. Obviously, Tamura, fractal, Gabor, and GLRLM are unsuitable for real-time systems since they require considerable much time for implementation. On the other hand, FOSH, GLCM, LBP, wavelet, and SAR were the fastest techniques because their processing time was less than 0.5 second. Space domain techniques, except radial averaging, recognized to be suitable for real-time purposes since they need processing time lower than that of our threshold, i.e. 0.5 second.

Many researchers reported that the combined feature models perform better than individual models. Hence, all of the real-time features were combined together to make two data sets, one for texture analysis methods and the other for space domain techniques. The combination process leads to produce data sets with large number of inputs so that the size of new texture analysis and space domain feature vectors was 125 (8 FOSH + 40 GLCM + 8 LBP + 64 wavelet + 5 SAR) and 17 (2 Farrell + 4

539 Lorentzian + 4 Gompertz + 6 statistical features + 1 Total number of pixels),
540 respectively. The large number of model inputs may leads to increase the execution
541 time and reduce the predictive accuracy. Using feature selection approaches such as
542 PCA, sensitivity analysis, genetic algorithms (GA), etc., these problems go away by
543 eliminating redundant features. In this study, genetic algorithm technique (GA) was
544 used for feature reduction as many researchers reported its suitability for this aim
545 (Leardi, 2000; Mollazade et al., 2012b). Table 5 shows the list of top texture analysis
546 and space domain features obtained by GA for apple, plum, tomato and mushroom.
547 Feature selection process considerably reduced the size of feature vectors so that the
548 size of texture analysis and time domain feature vectors was 10 and 2 for apple, 7 and
549 3 for plum, 5 and 4 for tomato, and 5 and 2 for mushroom, respectively. The wavelet
550 and modified Lorentzian function are superior compared to others since most of the
551 top features have been selected from the features of these techniques.
552 The ANFIS model with the selected texture analysis features gave the prediction
553 correlation coefficient of 0.872, 0.776, 0.853, and 0.827 for apple, plum, tomato, and
554 mushroom, respectively, which are slightly higher than that obtained by the ANFIS
555 models with individual texture analysis techniques (Tables 3 and 6). Regarding the
556 selected real-time space domain features, the same behavior has been observed so that
557 prediction correlation coefficient for apple, plum, tomato, and mushroom showed an
558 increase from 0.823 to 0.847, 0.754 to 0.762, 0.796 to 0.864, and 0.744 to 0.764,
559 respectively (Tables 4 and 7).
560
561 3.3. Fusion of selected real-time feature sets model
562 The real-time features selected from texture analysis and space domain techniques
563 (Table 5) were combined together in order to make a single feature set having the

benefits of two feature sets. Figure 7 presents the statistical measures of combined feature set model by ANFIS. Using the combined feature set model, the prediction accuracies of all the products were improved in comparison to the single real-time selected feature set models (Tables 6 and 7, and Figure 7). The correlation coefficient in prediction stage for tomato was highest (R_p=0.919) followed by mushroom (R_p=0.896), apple (R_p=0.887), and plum (R_p=0.790). This indicates that the integration of space domain and texture-based features considerably improved firmness/elasticity prediction for tomato and mushroom products but with a lesser degree of accuracy for apple and plum fruits. With the proposed features for laser induced backscattering imaging, the system is suitable to be implemented as a non-destructive technique in real-time machines to grade/sort horticultural products based on their mechanical properties. More efforts are needed to improve the capabilities of this system to meet the real-time requirements for monitoring different qualitative properties of horticultural produce. Works in this direction is in progress by authors.

Figure 5

Figure 6

Table 5

Table 6

Table 7

Figure 7

4. Conclusions

In this research an experimental analysis of a number of different texture analysis methods along with several space domain techniques was carried out for predicting mechanical properties of apple, plum, tomato and mushroom. Calibration models were developed by ANFIS that is an efficient artificial intelligent approach for

modeling. Texture analysis methods showed slightly better results than those of the space domain techniques when feature set of each technique was fed independently to the ANFIS. Results showed that combination of real-time features of texture analysis techniques was more effective than when they were used individually for predicting firmness/elasticity. Similar results were observed for the space domain techniques too. Feature selection process showed that not only it leads to a considerable reduction in the feature vectors but also improves the prediction accuracy of ANFIS models. Among all of the techniques used for feature extraction, wavelet transform and modified Lorentzian function are introduced as the best techniques for analysis of backscattering images. For all horticultural products in this research, it was found that integrating selected real-time features of both texture analysis and space domain techniques provides the best prediction results. The statistical performance for apple, tomato, and mushroom was in an acceptable range while real-time sensing of firmness for plum fruit was still poor. Future works should focus on the improving the accuracy and robustness of methods described in this research by applying the correction of light scattering distortion algorithms and methods that lead to increase signal to noise ratio.

Acknowledgments

The authors are grateful for the financial and technical support received from University of Tehran, University of Kurdistan, and Leibniz Institute for Agricultural Engineering Potsdam-Bornim (ATB) for this project.

References

613 Baranyai, L., Zude, M., 2009. Analysis of laser light propagation in kiwi fruit using
614 backscattering imaging and Monte Carlo simulation. Comput. Electron. Agric.
615 69, 33–39.
616 Bevk, M., Kononenko, I., 2002. A statistical approach to texture description of
617 medical images: A preliminary study. Proceedings of the 15th IEEE Symposium
618 on Computer-Based Medical Systems (CBMS 2002), 239-244.
619 Bharati, M.H., Liu, J.J., MacGregor, J.F., 2004. Image texture analysis: methods and
620 comparisons. Chemometr. Intell. Lab. 72, 57–71.
621 Choudhary, R., Paliwal, J., Jayas, D. S., 2008. Classification of cereal grains using
622 wavelet, morphological, colour, and textural features of non-touching kernel
623 images. Biosyst. eng. 99, 330-337.
624 Costa, A.F., Humpire-Mamani, G.E., Traina, A.J.M., 2012. An efficient algorithm for
625 fractal analysis of textures. In SIBGRAPI 2012: XXV Conference on Graphics,
626 Patterns, and Images, 39-46.
627 Garcia-Ramos, F.J., Valero, C., Homer, I., Ortiz-Canavate, J., Ruiz-Altisent, M.,
628 2005. Non-destructive fruit firmness sensors: a review. Span. J. Agric. Res. 3(1),
629 61-73.
630 Gonzalez, R.C., Woods, R.E., Eddins, S.L., 2004. Digital Image Processing using
631 MATLAB. Pearson Prentice Hall, New Jersey, USA.
632 Haralick, R.M., 1979. Statistical and structural approaches to texture. P. IEEE. 67,
633 786–804.
634 Haralick, R.M., Shanmugam, K., Dinstein, I., 1973. Textural features for image
635 classification. IEEE. T. Syst. Man. Cyb. 6, 610–621.
636 Jackman, P., Sun, D.W., 2012. Recent advances in image processing using image
637 texture features for food quality assessment. Tr. Food. Sci. Tec. 29(1), 35-43.

638 Jain, A., 1989. Fundamentals of Digital Image Processing. Prentice Hall International,
639 Englewood Cliffs, USA.
640 Jang, J.S.R., 1993. ANFIS: adaptive-network-based fuzzy inference system. IEEE. T.
641 Syst. Man. Cyb. 23(3), 665-685.
642 Leardi, R., 2000. Application of genetic algorithm-PLS for feature selection in
643 spectral data set. J. Chemometr. 14, 643-655.
644 Lu, R., 2004. Multispectral imaging for predicting firmness and soluble solids content
645 of apple fruit. Postharvest. Biol. Tec. 31, 147–157.
646 Mallat, S.G., 1989. A theory for multiresolution signal decomposition: the wavelet
647 representation. IEEE. T. Pattern. Anal. 11(7), 674-693.
648 Mireei, S.A., 2010. Nondestructive Determination of Effective Parameters on
649 Maturity of Mozafati and Shahani Date Fruits by NIR Spectroscopy Technique.
650 PhD Dissertation. Department of Mechanical Engineering of Agricultural
651 Machinery. University of Tehran. Iran. In Persian.
652 Mohsenin, N.N., 1986. Physical Properties of Plant and Animal Materials, Second
653 Edition Revised. Gordon and Breach Science, NY, USA.
654 Mollazade, K., Omid, M., Akhlaghian Tab, F., Mohtasebi, S.S. 2012a. Principles and
655 applications of light backscattering imaging in quality evaluation of agro-food
656 products: a review. Food. Bioprocess. Tech. 5(5), 1465-1485.
657 Mollazade, K., Omid, M., Akhlaghian Tab, F., Mohtasebi, S. S., Zude, M., 2012b.
658 Spatial mapping of moisture content in tomato fruits using hyperspectral imaging
659 and artificial neural networks. 4th International Workshop on Computer Image
660 Analysis in Agriculture, 09 - 11 July, Valencia, Spain.

661 Nicolai, B.M., Beullens, K., Bobelyn, E., Peirs, A., Saeys, W., Theron, K.I.,
662 Lammertyn, J., 2007. Nondestructive measurement of fruit and vegetable quality
663 by means of NIR spectroscopy: a review. Postharvest. Biol. Tec. 46, 99-118.
664 Noh, H.K., Lu, R., 2007. Hyperspectral laser-induced fluorescence imaging for
665 assessing apple fruit quality. Postharvest. Biol. Tec. 43, 193–201.
666 Ojala, T., Pietikäinen, M., Mäenpää, T., 2002. Multiresolution grey-scale and rotation
667 invariant texture classification with local binary patterns. IEEE. T. Pattern. Anal.
668 24(7), 971-987.
669 Omid, M., Mahmoudi, A., Omid, M.H., 2009. An intelligent system for sorting
670 pistachio nut varieties. Expert. Syst. Appl. 36, 11528–11535.
671 Omid, M., Mahmoudi, A., Omid, M.H., 2010. Development of pistachio sorting
672 system using principal component analysis (PCA) assisted artificial neural
673 network (ANN) of impact acoustics. Expert. Syst. Appl. 37, 7205–7212.
674 Peng, Y., Lu, R., 2005. Modeling multispectral scattering profiles for prediction of
675 apple fruit firmness. Trans. ASAE. 48(1), 235–242.
676 Peng, Y., Lu, R., 2006. Improving apple fruit firmness predictions by effective
677 correction of multispectral scattering images. Postharvest. Biol. Tec. 41, 266–
678 274.
679 Peng, Y., Lu, R., 2007. Prediction of apple fruit firmness and soluble solids content
680 using characteristics of multispectral scattering images. J. Food. Eng. 82, 142–
681 152.
682 Qin, J., Lu, R., 2006. Measurement of the optical properties of apple using
683 hyperspectral diffuse reflectance imaging. ASABE Paper No. 063037. St. Joseph,
684 Mich.: ASABE.

685 Qing, Z., Ji, B., Zude, M. 2007., Predicting soluble solid content and firmness in apple
686 fruit by means of laser light backscattering image analysis. J. Food. Eng. 82, 58–
687 67.
688 Qing, Z., Ji, B., Zude, M., 2008. Non-destructive analysis of apple quality parameters
689 by means of laser-induced light backscattering imaging. Postharvest. Biol. Tec.
690 48, 215–222.
691 Sarkar, A., Sharma, K., Sonak, R., 1997. A new approach for subset 2-D AR model
692 identification for describing textures. IEEE. T. Image. Process. 6(3), 407-413.
693 Sukissian, L., Kollias, S., Boutalis, Y., 1994. Adaptive classification of textured
694 images using linear prediction and neural networks. Signal. Process. 36, 209-232.
695 Tamura, H., Mori, S., Yamawaki, T., 1978. Textural features corresponding to visual
696 perception. IEEE Transactions on Systems, Man, and Cybernetics, 8, 460–472.
697 Tang, X., 1998. Texture information in run-length matrices. IEEE. T. Image. Process.
698 (7), 1602-1609
699 Zheng, C., Sun, D.W., Zheng, L., 2006. Recent applications of image texture for
700 evaluation of food qualities—a review. Tr. Food. Sci. Tec. 17, 113–128.
701 Zhu, B., Jiang, L., Luo, Y., Tao, Y., 2007. Gabor feature-based apple quality
702 inspection using kernel principal component analysis. J. Food. Eng. 81, 741,749.
703 Zude, M., 2009. Optical Monitoring of Fresh and Processed Agricultural Crops. CRC
704 Press, Boca Raton, FL, USA, 450 (pp. 391).
705
706

Table 1. Data set specification

Sample	Number of samples	Storage condition	Storage time	Mechanical property	Mean	Min	Max	Standard deviation
Apple	59 Pinova 68 Elstar	T: 2 ºC RH: 92±2 %	45 days	Firmness	59.85 (N/cm^2)	31.00 (N/cm^2)	84.50 (N/cm^2)	11.39 (N/cm^2)
Plum	180 Jojo 170 Tophit	T: 2 ºC RH: 92±2 %	20 days	Firmness	3.86 (N/cm^2)	0.09 (N/cm^2)	11.40 (N/cm^2)	2.41 (N/cm^2)
Tomato	200 Pannovy	T: 15±1 ºC RH: 92±2 %	30 days	Elasticity	0.43 (N/mm^2)	0.12 (N/mm^2)	1.75 (N/mm^2)	0.29 (N/mm^2)
Mushroom	200	T: 3±1 ºC RH: 92±2 %	14 days	Elasticity	1.53 (N/mm^2)	0.21 (N/mm^2)	4.92 (N/mm^2)	1.06 (N/mm^2)

Table 2. Available texture features measured by statistical techniques for each backscattering image

1st order statistics of image histogram and local binary pattern		Grey level co-occurrence matrix		Grey level run length matrix	
Feature name	Formula*	Feature name	Formula**	Feature name	Formula***
Mean grey level	$\mu = \sum_{i=0}^{L-1} z_i p(z_i)$	Contrast	$\sum_{i,j} \lvert i-j \rvert^2 p(i,j)$	Short run emphasis (SRE)	$\frac{\sum_{i=1}^{N_g}\sum_{j=1}^{N_r} \frac{r(i,j)}{j^2}}{\sum_{i=1}^{N_g}\sum_{j=1}^{N_r} r(i,j)}$
Standard deviation	$\sigma = \sqrt{\sum_{i=0}^{L-1} (z_i-\mu)^2 p(z_i)}$	Correlation	$\sum_{i,j} \frac{(i-\mu i)(j-\mu j)p(i,j)}{\sigma_i \sigma_j}$	Long run emphasis (LRE)	$\frac{\sum_{i=1}^{N_g}\sum_{j=1}^{N_r} j^2 r(i,j)}{\sum_{i=1}^{N_g}\sum_{j=1}^{N_r} r(i,j)}$
Smoothness	$1 - 1/(1+\sigma^2)$	Uniformity	$\sum_{i,j} p(i,j)^2$	Grey level non-uniformity (GLNU)	$\frac{\sum_{i=1}^{N_g}(\sum_{j=1}^{N_r} r(i,j))^2}{\sum_{i=1}^{N_g}\sum_{j=1}^{N_r} r(i,j)}$
Skewness	$\frac{1}{\sigma^3}\sum_{i=0}^{L-1}(z_i-\mu)^3 p(z_i)$	Homogeneity	$\sum_{i,j} \frac{p(i,j)}{1+\lvert i-j \rvert}$	Run length non - uniformity (RLNU)	$\frac{\sum_{i=1}^{N_r}(\sum_{j=1}^{N_g} r(i,j))^2}{\sum_{i=1}^{N_g}\sum_{j=1}^{N_r} r(i,j)}$
Uniformity (energy)	$\sum_{i=0}^{L-1} P^2(z_i)$	Entropy	$-\sum_{i,j} p(i,j) log p(i,j)$	Run percentage (RP)	$\frac{\sum_{i=1}^{N_g}\sum_{j=1}^{N_r} r(i,j)}{n_p}$
Entropy	$-\sum_{i=0}^{L-1} p(z_i)\log_2 p(z_i)$	Maximum of probability	$Max\ (p(i,j))$	Low grey level run emphasis (LGRE)	$\frac{\sum_{i=1}^{N_g}\sum_{j=1}^{N_r} \frac{r(i,j)}{i^2}}{\sum_{i=1}^{N_g}\sum_{j=1}^{N_r} r(i,j)}$
Kurtosis (4th moment)	$\frac{1}{\sigma^4}\sum_{i=0}^{L-1}(z_i-\mu)^4 p(z_i)$	Dissimilarity	$\sum_{i,j} \lvert i-j \rvert p(i,j)$	High grey level run emphasis (HGRE)	$\frac{\sum_{i=1}^{N_g}\sum_{j=1}^{N_r} r(i,j).i^2}{\sum_{i=1}^{N_g}\sum_{j=1}^{N_r} r(i,j)}$
Coefficient of variation	$\frac{\sigma}{\mu}$	Cluster shade	$\sum_{i,j} ((i-\mu i)+(j-\mu j))^3 p(i,j)$	Short run low grey level emphasis (SRLGE)	$\frac{\sum_{i=1}^{N_g}\sum_{j=1}^{N_r} \frac{r(i,j)}{i^2.j^2}}{\sum_{i=1}^{N_g}\sum_{j=1}^{N_r} r(i,j)}$
		Cluster prominence	$\sum_{i,j} ((i-\mu i)+(j-\mu j))^4 p(i,j)$	Short run high grey level emphasis (SRHGE)	$\frac{\sum_{i=1}^{N_g}\sum_{j=1}^{N_r} \frac{r(i,j).i^2}{j^2}}{\sum_{i=1}^{N_g}\sum_{j=1}^{N_r} r(i,j)}$
		Variance	$\sum_{i,j} (i-\mu i)^2 p(i,j)$	Long run low grey level emphasis (LRLGE)	$\frac{\sum_{i=1}^{N_g}\sum_{j=1}^{N_r} \frac{r(i,j).j^2}{i^2}}{\sum_{i=1}^{N_g}\sum_{j=1}^{N_r} r(i,j)}$
				Long run high grey level emphasis (LRHGE)	$\frac{\sum_{i=1}^{N_g}\sum_{j=1}^{N_r} r(i,j).i^2.j^2}{\sum_{i=1}^{N_g}\sum_{j=1}^{N_r} r(i,j)}$

* μ_n, z_i, $p(z_i)$, and L represent mean n[th] moment, random variable related to intensity, normalized histogram of intensity levels, and number of possible intensity levels, respectively.

** is standard deviation, represents the mean, and $p(i, j)$ is grey level co-occurrence matrix.

*** $r(i, j)$, N_g, N_r, and n_p are run length matrix, number of grey levels in an image, number of run lengths, and sum of image pixels, respectively.

Table 3. The characteristics and statistical measures of the best models of ANFIS for predicting firmness/elasticity of some horticultural products by different texture analysis techniques

Product	Texture analysis technique	Type of mf		Number of Input mf	Optimization method	Calibration		Prediction	
		Input	Output			RMSECV	R_c	RMSEP	R_p
Apple	FOSH	Triangular	Linear	5	Hybrid	4.423	0.929	8.583	0.861
	GLCM	Trapezoidal	Linear	3	Hybrid	7.080	0.783	14.229	0.736
	GLRLM	Bell-shaped	Linear	4	Hybrid	2.357	0.979	12.119	0.701
	LBP	Triangular	Linear	4	Hybrid	3.129	0.962	14.825	0.512
	Wavelet	Trapezoidal	Linear	3	Hybrid	6.670	0.846	10.320	0.825
	Gabor	Gaussian	Constant	5	Hybrid	6.377	0.861	13.587	0.637
	Tamura	Trapezoidal	Linear	4	Hybrid	5.860	0.861	10.398	0.846
	Fractal	Sigmoid	Linear	3	Hybrid	5.954	0.869	8.998	0.826
	SAR	Bell-shaped	Constant	4	Hybrid	7.652	0.772	13.814	0.706
Plum	FOSH	Sigmoid	Linear	5	Hybrid	2.650	0.671	2.708	0.722
	GLCM	Triangular	Linear	5	Hybrid	2.091	0.623	3.325	0.659
	GLRLM	Sigmoid	Linear	5	Hybrid	1.862	0.686	2.044	0.697
	LBP	Trapezoidal	Constant	4	Hybrid	2.603	0.583	2.318	0.687
	Wavelet	Triangular	Linear	5	Hybrid	1.993	0.589	2.607	0.554
	Gabor	Trapezoidal	Linear	2	Hybrid	3.869	0.544	4.018	0.606
	Tamura	Sigmoid	Linear	5	Hybrid	1.809	0.692	2.444	0.712
	Fractal	Triangular	Linear	3	Hybrid	2.470	0.649	2.314	0.725
	SAR	Gaussian	Constant	4	Hybrid	1.968	0.645	1.722	0.757
Tomato	FOSH	Bell-shaped	Linear	3	Hybrid	0.325	0.648	0.356	0.678
	GLCM	Sigmoid	Linear	5	Hybrid	0.284	0.621	0.277	0.718
	GLRLM	Gaussian	Linear	4	Hybrid	0.268	0.621	0.344	0.675
	LBP	Gaussian	Linear	4	Hybrid	0.246	0.603	0.298	0.692
	Wavelet	Gaussian	Constant	4	Hybrid	0.258	0.677	0.237	0.795
	Gabor	Sigmoid	Linear	5	Hybrid	0.221	0.722	0.259	0.857
	Tamura	Gaussian	Linear	4	Hybrid	0.298	0.731	0.219	0.832
	Fractal	Triangular	Linear	4	Hybrid	0.295	0.685	0.339	0.791
	SAR	Sigmoid	Linear	3	Hybrid	0.256	0.740	0.425	0.706
Mushroom	FOSH	Gaussian	Constant	5	Hybrid	0.727	0.734	0.988	0.780
	GLCM	Sigmoid	Linear	4	Hybrid	0.789	0.721	1.331	0.780
	GLRLM	Sigmoid	Constant	4	Hybrid	0.791	0.699	0.782	0.779
	LBP	Bell-shaped	Linear	5	Hybrid	0.331	0.951	1.012	0.739
	Wavelet	Bell-shaped	Linear	3	Hybrid	0.832	0.724	1.477	0.746
	Gabor	Trapezoidal	Linear	4	Hybrid	0.695	0.742	0.994	0.788
	Tamura	Triangular	Linear	3	Hybrid	0.937	0.710	0.696	0.839
	Fractal	Triangular	Constant	5	Hybrid	0.643	0.803	1.005	0.780
	SAR	Bell-shaped	Constant	2	Hybrid	1.516	0.619	1.195	0.717

Table 4. The characteristics and statistical measures of the best models of ANFIS for predicting firmness/elasticity of some horticultural products by different space domain techniques

Product	Texture analysis technique	Type of mf		Number of Input mf	Optimization method	Calibration		Prediction	
		Input	Output			RMSECV	R_c	RMSEP	R_p
Apple	Total number of pixels	Trapezoidal	Linear	5	Hybrid	14.259	0.369	20.636	0.506
	Statistical features	Bell-shaped	Constant	4	Hybrid	7.961	0.720	11.883	0.761
	Radial averaging	Trapezoidal	Linear	4	Hybrid	7.621	0.861	11.254	0.789
	Lorentzian	Gaussian	Linear	5	Hybrid	8.209	0.755	14.536	0.753
	Gompertz	Sigmoid	Linear	3	Hybrid	11.512	0.497	15.831	0.562
	Farrel	Gaussian	Linear	4	Hybrid	8.671	0.672	10.332	0.823
Plum	Total number of pixels	Triangular	Constant	5	Hybrid	3.342	0.317	4.544	0.536
	Statistical features	Bell-shaped	Linear	4	Hybrid	1.682	0.723	2.195	0.754
	Radial averaging	Trapezoidal	Constant	4	Hybrid	2.031	0.593	2.408	0.630
	Lorentzian	Trapezoidal	Constant	4	Hybrid	2.568	0.252	4.496	0.411
	Gompertz	Triangular	Linear	2	Hybrid	2.544	0.457	3.056	0.450
	Farrel	Triangular	Constant	5	Hybrid	2.461	0.413	2.206	0.710
Tomato	Total number of pixels	Trapezoidal	Constant	2	Hybrid	0.471	0.689	0.374	0.668
	Statistical features	Bell-shaped	Linear	3	Hybrid	0.197	0.841	0.278	0.792
	Radial averaging	Gaussian	Linear	4	Hybrid	0.143	0.911	0.257	0.795
	Lorentzian	Triangular	Linear	4	Hybrid	0.186	0.811	0.360	0.789
	Gompertz	Triangular	Linear	2	Hybrid	0.197	0.755	0.289	0.773
	Farrel	Trapezoidal	Constant	2	Hybrid	0.254	0.834	0.345	0.796
Mushroom	Total number of pixels	Bell-shaped	Constant	4	Hybrid	1.123	0.284	1.584	0.499
	Statistical features	Triangular	Linear	4	Hybrid	0.861	0.772	0.968	0.744
	Radial averaging	Trapezoidal	Linear	3	Hybrid	0.587	0.843	0.841	0.827
	Lorentzian	Triangular	Linear	5	Hybrid	1.175	0.352	1.257	0.627
	Gompertz	Bell-shaped	Constant	3	Hybrid	1.219	0.381	0.999	0.642
	Farrel	Gaussian	Linear	4	Hybrid	0.837	0.637	1.062	0.701

Table 5. The list of top real-time features selected by GA for predicting mechanical properties of different type of horticultural products

Apple		Plum		Tomato		Mushroom	
Texture analysis	Space domain statistics	Texture analysis	Space domain statistics	Texture analysis	Space domain statistics	Texture analysis	Space domain statistics
FOSH (skewness)	Farrell (μ_s')	LBP (kurtosis)	Lorentzian (c)	Wavelet (mean-diagonal-2)	Lorentzian (b)	GLCM (Contrast-45º)	Farrell (μ_a)
FOSH (entropy)	Lorentzian (b)	Wavelet (mean-vertical-1)	Gompertz (α)	Wavelet (mean-vertical-3)	Lorentzian (d)	GLCM (Contrast-90º)	Lorentzian (c)
FOSH (coefficient of variation)		Wavelet (mean-horizontal-2)	Statistical features (mean)	Wavelet (mean-vertical-4)	Gompertz (β)	Wavelet (mean-vertical-2)	
Wavelet (standard deviation-horizontal-4)		Wavelet (mean-vertical-2)		SAR (θ_3)	Statistical features (min)	Wavelet (mean-diagonal-3)	
Wavelet (energy-horizontal-1)		Wavelet (mean-diagonal-2)		SAR (θ_4)		Wavelet (mean-vertical-4)	
Wavelet (energy-horizontal-4)		SAR (θ_1)					
Wavelet (entropy-horizontal-1)		SAR (θ_2)					
Wavelet (entropy-approximation-3)							
Wavelet (entropy-horizontal-4)							
Wavelet (entropy-vertical-1)							

FOSH: First order statistics of image histogram, LBP: Local Binary pattern, SAR: Simultaneous autoregressive model, GLCM: Grey level co-occurrence matrix

Table 6. The characteristics and statistical measures of the best models of ANFIS for predicting firmness/elasticity of some horticultural products by selected features from real-time texture analysis techniques

Product	Type of mf		Number of Input mf	Optimization method	Calibration		Prediction	
	Input	Output			RMSECV	R_c	RMSEP	R_p
Apple	Trapezoidal	Constant	4	Hybrid	6.288	0.907	12.474	0.872
Plum	Trapezoidal	Linear	4	Hybrid	1.948	0.724	3.287	0.776
Tomato	Triangular	Linear	2	Hybrid	0.242	0.767	0.203	0.853
Mushroom	Trapezoidal	Constant	4	Hybrid	0.783	0.722	0.896	0.872

Table 7. The characteristics and statistical measures of the best models of ANFIS for predicting firmness/elasticity of some horticultural products by selected features from real-time space domain techniques

Product	Type of mf		Number of Input mf	Optimization method	Calibration		Prediction	
	Input	Output			RMSECV	R_c	RMSEP	R_p
Apple	Trapezoidal	Linear	5	Hybrid	10.940	0.723	10.989	0.847
Plum	Triangular	Linear	3	Hybrid	2.249	0.668	1.687	0.762
Tomato	Sigmoid	Linear	5	Hybrid	0.179	0.863	0.260	0.864
Mushroom	Trapezoidal	Constant	2	Hybrid	0.870	0.603	1.278	0.764

Figure captions

Click here to download Figure: Figure captions.docx

Figure 1. Wavelet decomposition of backscattering image of a tomato sample at 660 nm using a fourth-order Daubechies mother wavelet (Db4)

Figure 2. Magnitude of Gabor wavelet transform obtained for backscattering image of a tomato sample at 660 nm in different directions and frequencies

Figure 3. The process of extracting the fractal features from backscattering image of a tomato sample at 660 nm by segmentation-based fractal texture analysis (SFTA) algorithm

Figure 4. The selection pattern of neighborhoods for a pixel at position s in the simultaneous autoregressive (SAR) model. The neighboring pixels are left, left-up, up, and right-up.

Figure 5. Processing time required to extract features from backscattering images of horticultural products by different texture analysis techniques

Figure 6. Processing time required to extract features from backscattering images of horticultural products by different space domain techniques

Figure 7. Results of predicting firmness/elasticity by fusion the selected features from real-time texture analysis and space domain feature sets for A. Apple, B. Plum, C. Tomato, and D. Mushroom. Red and blue dots represent the calibration and prediction data, respectively.

Figure 1

Click here to download Figure: Figure 1.docx

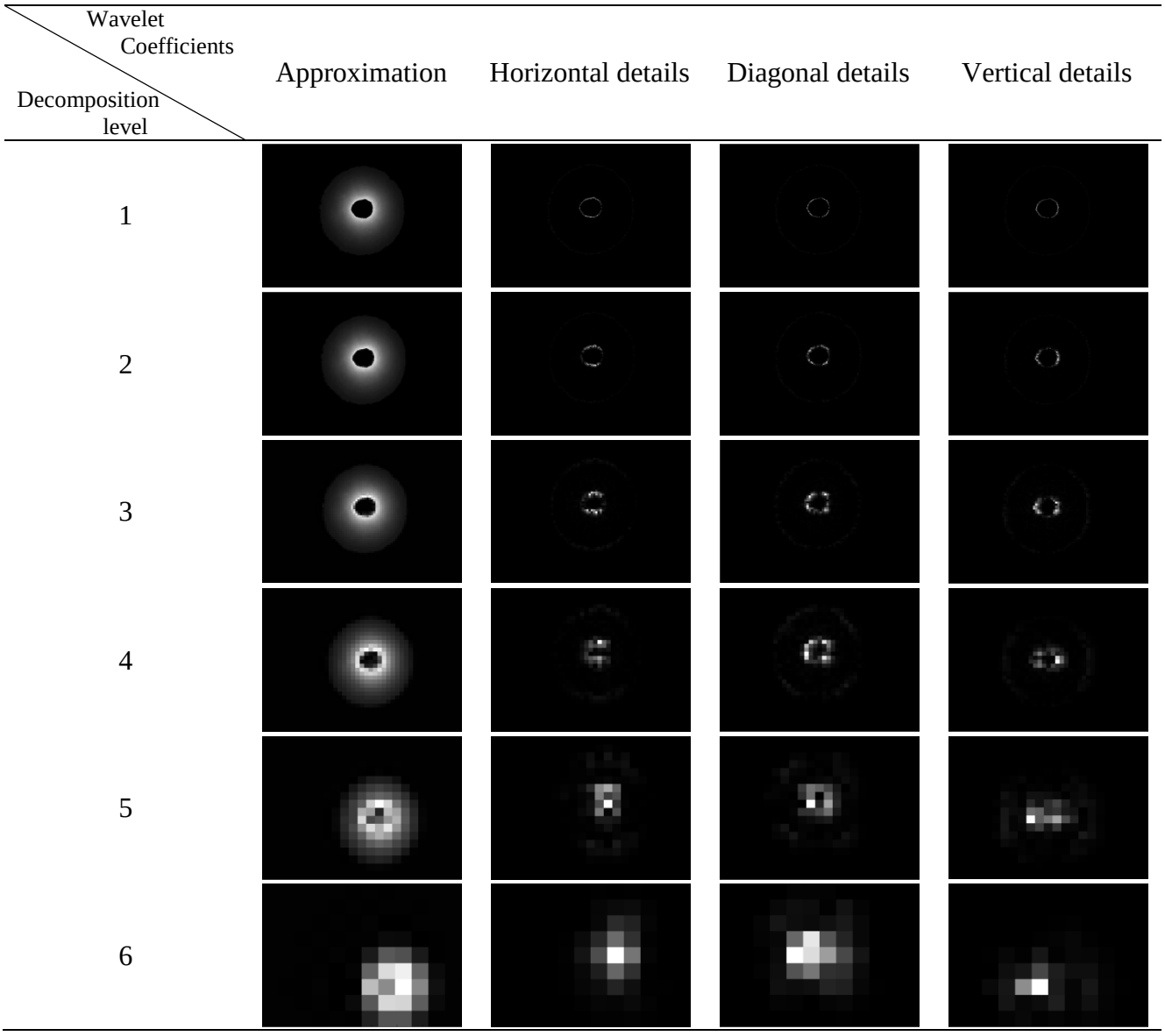

Figure 2

Click here to download Figure: Figure 2.doc

Direction (radian) / Frequency (Hz)	0	π/4	π/2	3π/4
0.1768	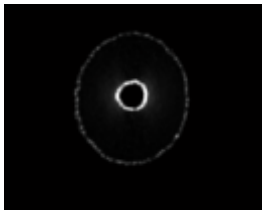	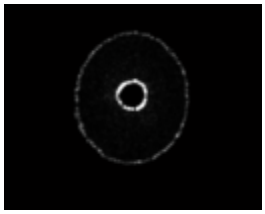	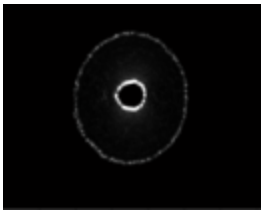	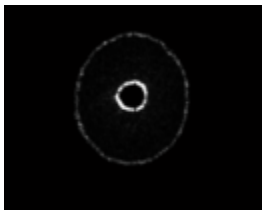
0.2500	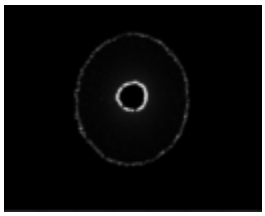	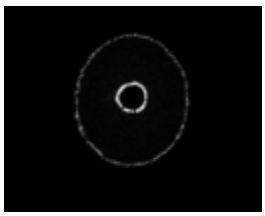	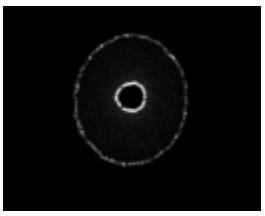	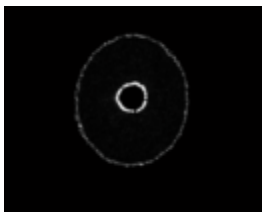
0.3536	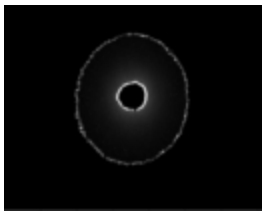	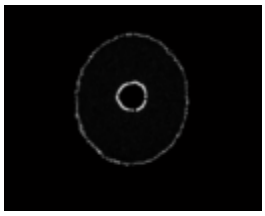	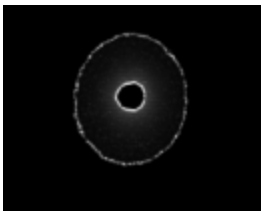	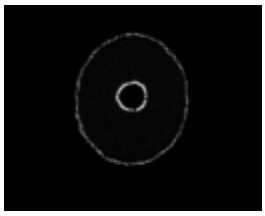
0.5000	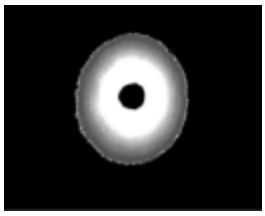	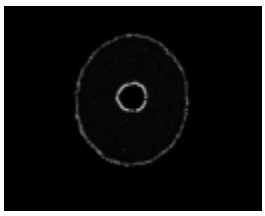	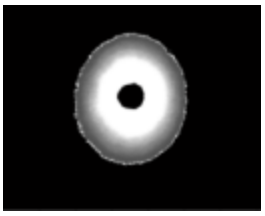	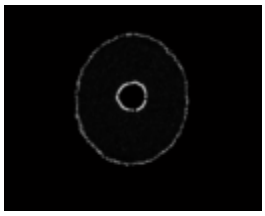

Figure 3

Click here to download Figure: Figure 3.docx

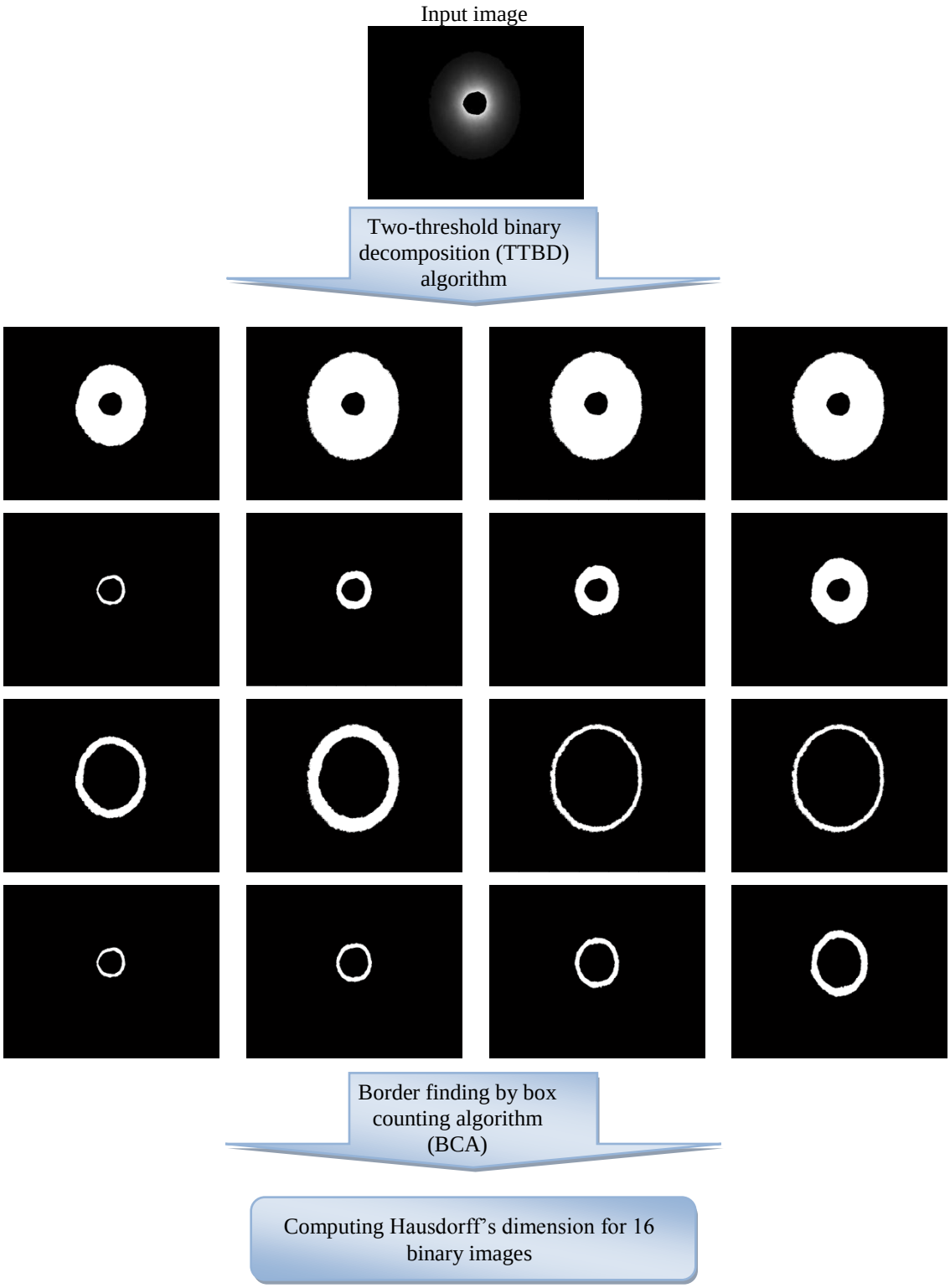

Figure 4

Click here to download Figure: Figure 4.docx

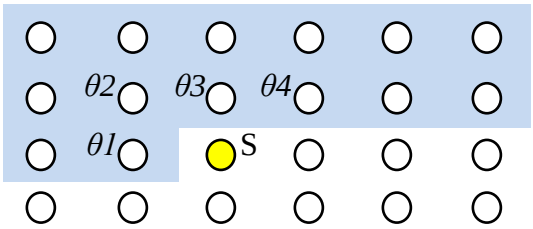

Figure 5

Click here to download Figure: Figure 5.docx

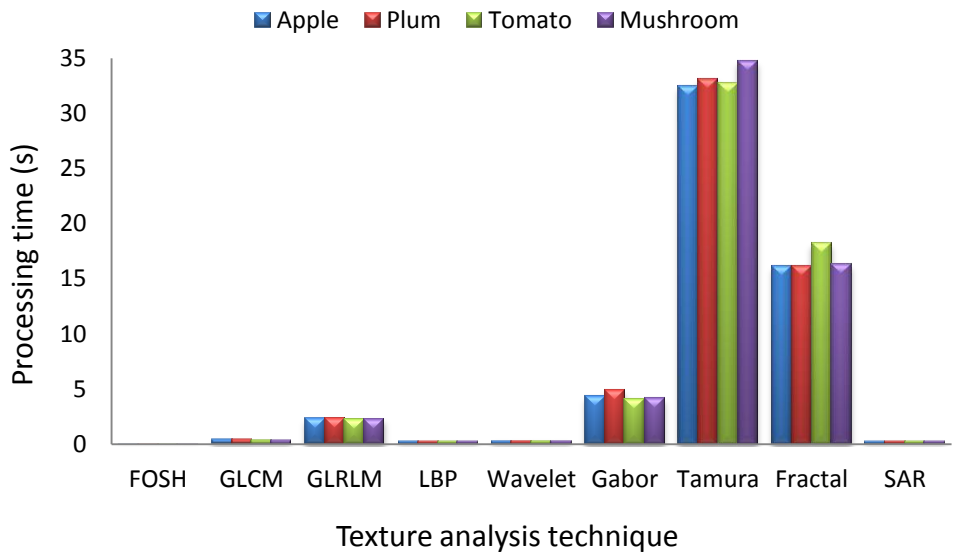

Figure 6

Click here to download Figure: Figure 6.docx

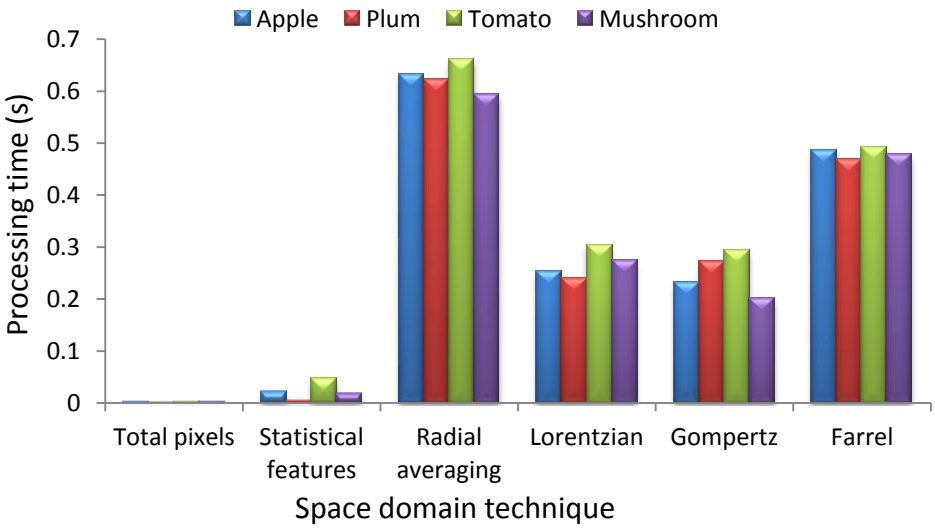

Figure 7

Click here to download Figure: Figure 7.docx